Sensors and Materials, Vol. 30, No. 1 (2018) 101–109
MYU Tokyo

S & M 1476

Displacement Measurement Realized by Near-field Coupling between Multiple Coils

Shujing Su,[1,2#] Lei Zhang,[1,2#] Yanjie Guo,[1,2]
Fei Lu,[1,2] Qiulin Tan,[1,2*] and Jijun Xiong,[1,2]

[1]Key Laboratory of Instrumentation Science & Dynamic Measurement (North University of China), Ministry of Education, North University of China, Tai Yuan 030051, China
[2]Science and Technology on Electronic Test and Measurement Laboratory, North University of China, Tai Yuan 030051, China

(Received May 22, 2017; accepted August 8, 2017)

Keywords: displacement sensing, near-field coupling, ADS simulation, coupling model, tentative experiment

A displacement-sensing scheme is presented herein by utilizing near-field coupling between multiple coils. The sensing system consists of the stationary part and removable sensor tag. The change in the relative position between the stationary part and the sensor tag can result in the variation of characteristic frequencies, which can be retrieved from the impedance of the reader antenna on the side of the stationary part. The lumped model of the system is established for theoretical analysis, and the results of the analysis were verified by electromagnetic simulation. A prototype of the system was fabricated by printed circuit board (PCB) technology to carry out tentative experiments, the results of which were used to verify the findings of the theoretical analysis and simulation. The results of the experiment conducted in the lab demonstrated that the sensor is capable of the contactless measurement of displacement from 3 to 10 mm with a considerable average sensitivity of 1.5 MHz/mm.

1. Introduction

Displacement measurement has many applications, such as in civil engineering,[1–3] automation, and industrial monitoring.[4–8] A variety of sensing techniques have been developed for contactless displacement sensing in the past decades, for example, the eddy current, capacitive, optical, and inductive displacement sensors.[4,9,10] Optical sensors have better accuracy, stability, and linearity than all other sensors, but they are usually bulky and costly owing to the requirements of a laser, lens, and electronic components. The capacitive sensor can achieve exceptionally high resolution and stability, and yet it is quite sensitive to dust and pollutants in the air-gap or electrode surface.[11] Eddy current and inductive sensors are inherently robust, low in cost, high in performance, and insensitive to environmental contaminants, making them suitable for most industrial applications.[9]

*Corresponding author: e-mail: tanqiulin@nuc.edu.cn
#These authors contributed equally to this work.
http://dx.doi.org/10.18494/SAM.2018.1632

ISSN 0914-4935

However, eddy current sensors are sensitive to temperature because of the high temperature coefficient of metal resistivity, and inductive sensors have shortcomings due to the temperature-dependent permeability of the target material and the presence of magnetic hysteresis.[11] These drawbacks make eddy current and inductive sensors an unsuitable choice for precise displacement measurement in high-temperature environments. Therefore, novel schemes for contactless displacement measurement in harsh environments must be developed.

In this paper, a scheme for displacement sensing by near-field coupling between multiple inductor-capacitor (LC) tanks is proposed. Although the same model had already been used to enhance the readout signal strength of an LC resonant sensor[12] and the design of a passive multiparameter LC sensor,[13] it has not been used to perform displacement sensing. By theoretical analysis and simulation, the feasibility of the scheme was demonstrated. The displacement of the sensor tag can be measured by tracking the maximum or minimum frequency extracted from the impedance characteristic parameters (phase, real part, etc.) of the reader coil. A prototype of the sensing system was built and tested to validate the feasibility of the method experimentally, and considerable sensitivity was obtained within the measurement range of 10 mm.

2. Theoretical Analysis of Model

The diagrammatic sketch of a multiple-LC-tanks measurement model and lumped circuit model of the system are illustrated in Fig. 1. As shown in Fig. 1(a), the sensing system consists of three planar spiral coils, and two of which constitute the stationary part, which is also the signal transmitter and receiver port of the system, while the remaining coil plays the role of a removable sensor tag. By extracting a certain impedance characteristic parameter, the variation of sensor tag displacement can be detected with high resolution. As illustrated in Fig. 1(b), the components on the right (L_r, R_r) correspond to the lumped parameters of the reader antenna, the components in the middle (L_t, R_t, and C_t) denote the lumped parameters of the transmitting coil, and the components on the left (L_s, R_s, and C_s) represent the discrete parameters of the sensor tag. Here, k_{rt}, k_{rs}, and k_{st} are the coupling coefficients between the reader antenna and transmitting coil, the reader antenna and sensor tag, and the transmitting coil and sensor tag, respectively, and are used to represent the magnetic coupling strength between these coils.

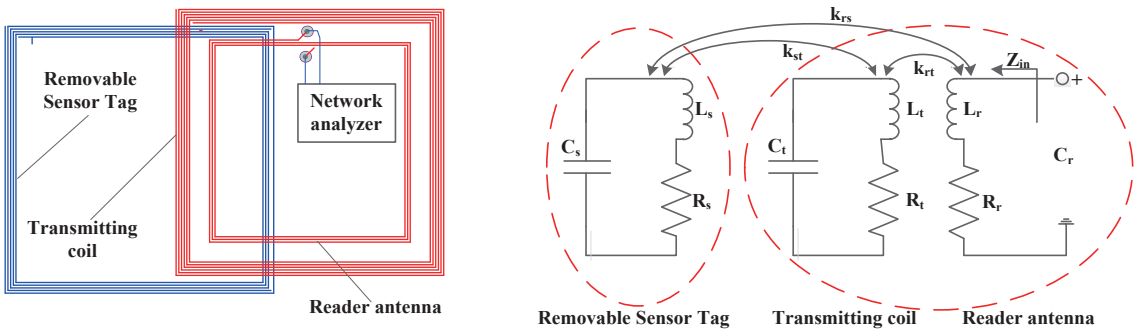

Fig. 1. (Color online) (a) Diagrammatic sketch of the sensing system and (b) its lumped circuit model.

For the reader antenna, L_r is the equivalent inductance and R_r is its inherent resistance. It should be noted that the parasitic capacitance of the antenna is ignored in the model to simplify the theoretical analysis. Accordingly, L_t is the equivalent inductance of the transmitting coil, R_t is its inherent resistance and C_t is the parasitic capacitance. With regard to the sensor tag, L_s, R_s, and C_s are the inductance, inherent resistance, and parasitic capacitance, respectively. As illustrated in the model, the transmitting coil and sensor tag can be considered as LC tanks with specific resonant frequencies. The parasitic capacitance, C_{par}, is given by[14]

$$C_{par} = C_1 + C_2 = (\alpha\varepsilon_{r1} + \beta\varepsilon_{r2})\varepsilon_0 \frac{t}{s} l_g, \tag{1}$$

where α and β are empirical constants with the values of 0.9 and 0.1, respectively. ε_{r1} and ε_{r2} are, respectively, the relative dielectric constants of the covering layer and the substrate material, and ε_0 is the vacuum permittivity. t is the thickness of the metal conductor of the inductance coil, s is the spacing of wire conductors, and l_g is the total length of wire clearance, as shown in Fig. 2.

In order to analyze the system theoretically, the transformer network theory and Kirchhoff's law are used to list loop equations. The input impedance Z_{in} referencing the ports of the reader antenna is derived as[13]

$$\begin{aligned} Z_{in} = R_r + jwL_r + jwk_{rt}\sqrt{L_rL_t}\frac{-w^2k_{rs}k_{st}L_r\sqrt{L_tL_s} - jwk_{rt}\sqrt{L_rL_t}Z_s}{Z_tZ_s + w^2k_{st}^2L_tL_s} \\ + jwk_{rs}\sqrt{L_rL_s}\frac{-w^2k_{rt}k_{st}L_r\sqrt{L_tL_r} - jwk_{rs}\sqrt{L_rL_s}Z_t}{Z_tZ_s + w^2k_{st}^2L_tL_s} \end{aligned}. \tag{2}$$

In Eq. (2), Z_t and Z_s are the series impedance of the transmitting coil and sensor tag, respectively, and can be given as

$$Z_t = R_t + jwL_t + \frac{1}{jwC_t}, \tag{3}$$

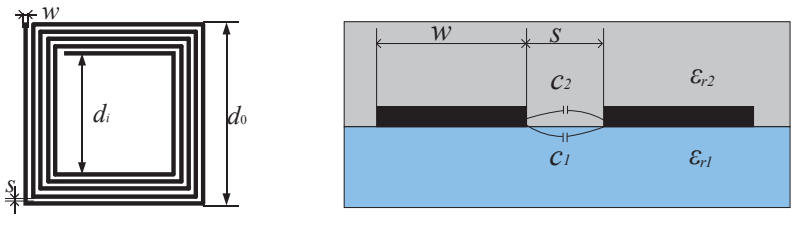

(a) (b)

Fig. 2. (Color online) (a) Schematic diagram of square plane spiral parameters and (b) the model of parasitic capacitance.

$$Z_s = R_s + jwL_s + \frac{1}{jwC_s}. \tag{4}$$

The phase expression is shown as

$$\angle Z_{in} = \arctan\left(\frac{Im\{Z_{in}\}}{Re\{Z_{in}\}}\right). \tag{5}$$

The specific expression for Z_{in} is cumbersome, so MATLAB software is used to perform the mathematical calculation. The expression Z_{in} is a complex variable with amplitude (real part) and phase (imaginary part), whereas the phase of Z_{in} is particularly investigated in this study. At the side of the stationary part, the relative position between the reader antenna and transmitting coil is permanent so the coupling coefficient between them, k_{rt}, is constant. For the sake of further simplification of the analysis, we assumed that the coupling coefficient between the antenna and sensor tag, k_{rs}, is also a constant in the next analysis.

The frequency, f_{min}, is usually recorded as it is related to the resonant frequency of the sensor through the following relationship:[15]

$$f_{min} = f_0(1 + \frac{k^2}{4} + \frac{1}{8Q^2}), \tag{6}$$

where f_{min} and Q are the resonant frequency and the quality factor of the sensor, respectively, and f_0 is a constant defined by L_s and C_s. In the actual test, the sensor has a high Q-factor when the coupling coefficient k is changed slightly and the resonant frequency is almost constant. It is reasonable to put forward this hypothesis because the coupling link between these two coils has almost no influence on the accuracy of peak frequencies extracted from phase of Z_{in}, where the software advanced designer system (ADS) is used for the simulation, as illustrated in Fig. 3, and the parameters of the simulation are identical to the parameters in the model.

In Fig. 3, there are two negative peak frequencies corresponding to the resonant characteristic of the two LC tanks (the transmitting coil and sensor tag). When k_{rs} increases from 0.22 to 0.3, the two negative peak frequencies vary negligibly, so we focus on investigating the influence of k_{st} on the extracted peak frequencies. A planar spiral inductor coupling model with multiple coils was built to analyze the influence of k_{st}, as shown in Fig. 3(a). The fundamental coupling model between two single coils is presented in Fig. 3(b). When two coils are directly opposite each other, the mutual inductance between two coils can be expressed as

$$M(a,b,L) = \mu_0 \sqrt{ab}\left[\left(\frac{2}{k} - k\right)K(k) - \frac{2}{k}E(k)\right], \tag{7}$$

where

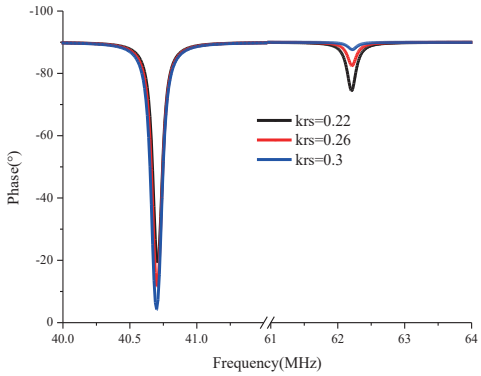

Fig. 3. (Color online) Theoretical analysis results for the influence of k_{rs} on peak frequencies. The discrete parameters setup for the analysis is $k_{st} = 0.4$, $k_{rt} = 0.351$, $R_r = 0.5329$ Ω, $R_t = R_s = 1.73$ Ω, $L_r = 0.43$ μH, $L_t = L_s = 2.87$ μH, and $C_t = C_s = 3.8$ pF.

$$k = \left(\frac{4ab}{(a+b)^2 + L^2} \right)^{\frac{1}{2}}. \tag{8}$$

$K(k)$ and $E(k)$ are the first and second kinds of elliptic integral, respectively. μ_0 is the vacuum permeability. a is the radius/side length of a circle/square. L is the vertical distance between two coils. The mutual inductance between the transmitting coil and removable sensor tag can be represented as

$$M_{st} = \sum_{i=1}^{i=N_s} \sum_{j=1}^{j=N_t} M(a_i, b_j, L), \tag{9}$$

where

$$a_i = \frac{d_{out\_s}}{2} - (N_s - i)(W + S), \tag{10}$$

$$b_j = \frac{d_{out\_t}}{2} - (N_t - j)(W + S). \tag{11}$$

N_s and N_t are the number of coil turns of the sensor tag and transmitting coil, d_{out_s} and d_{out_t} are the lengths of their outermost segments, and a_i and b_j are the side length of each turn, respectively. W and S are the conductor width and conductor spacing, respectively. Hence the coupling coefficient can be given as

$$k_{st} = \frac{M_{st}}{\sqrt{L_s L_t}}. \tag{12}$$

Here, L_s and L_t are the inductive coil of the sensor tag and transmitting coil, respectively. The coupling coefficients k_{rs} and k_{rt} can be analyzed in the same way.

Systematic analysis is implemented under the conditions of $f_{0t} < f_{0s}$, $f_{0t} > f_{0s}$, and $f_{0t} = f_{0s}$ corresponding to $N_t > N_s$, $N_t < N_s$, and $N_t = N_s$ with the other parameters unchanged. f_{0s} and f_{0t} are the self-resonant frequencies of the sensor tag and transmitting coil. It is shown in Fig. 4 that the lower and higher peak frequencies decrease when L increases. Practically, the change in k_{st} can reflect the change in the relative positions of the sensor tag coil and the stationary part, so the peak frequencies are displacement dependent. On the basis of the above analysis, if one of the peak frequencies can be tracked, the variation in the relative displacement between them can be detected.

As shown in Figs. 4(a)–4(c), the higher peak frequencies change more than the lower ones, so the higher peak frequencies were chosen as tracking objects. From Fig. 4(d), it can be seen that when $f_{0t} > f_{0s}$, the higher peak frequency decreases by 6.08 MHz. When $f_{0t} < f_{0s}$, the higher peak frequency decreases by 7.02 MHz. Under the condition of $f_{0t} = f_{0s}$, the higher peak frequency decreases by 7.24 MHz. By comparing the data described above, it can be seen that greater sensitivity can be obtained if the self-resonant frequencies of the transmitting coil and the tag are equal.

3. Simulation and Experiment with the Model

In order to verify the theoretical analysis, the electromagnetic simulation software ADS was used in the layout mode. Here, all coils were designed as square planar spiral coils, and the transmitting coil and reader antenna were placed coaxially in the same plane. The sensor tag coil was designed with identical dimensions to the transmitting coil and they were placed in positive alignment. The distance L between the transmitting coil and tag coil varies in layout simulation, and the higher peak frequency was tracked. It is shown in Fig. 5 that the frequency decreases from 66.7 to 56.3 MHz when L increases from 3 to 10 mm. The simulated parameters of the sensor tag and reader antenna are listed in Table 1; they are the same as the parameters in the model. When the distance between the transmitting coil and sensor tag is 3 mm, according

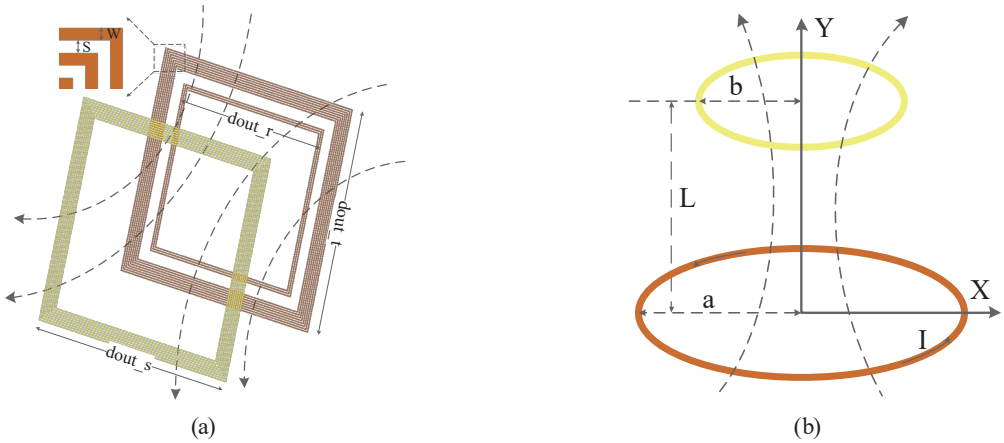

(a) (b)

Fig. 4. (Color online) (a) Schematic of planar spiral inductor mutual coupling and (b) basic coil unit coupling model.

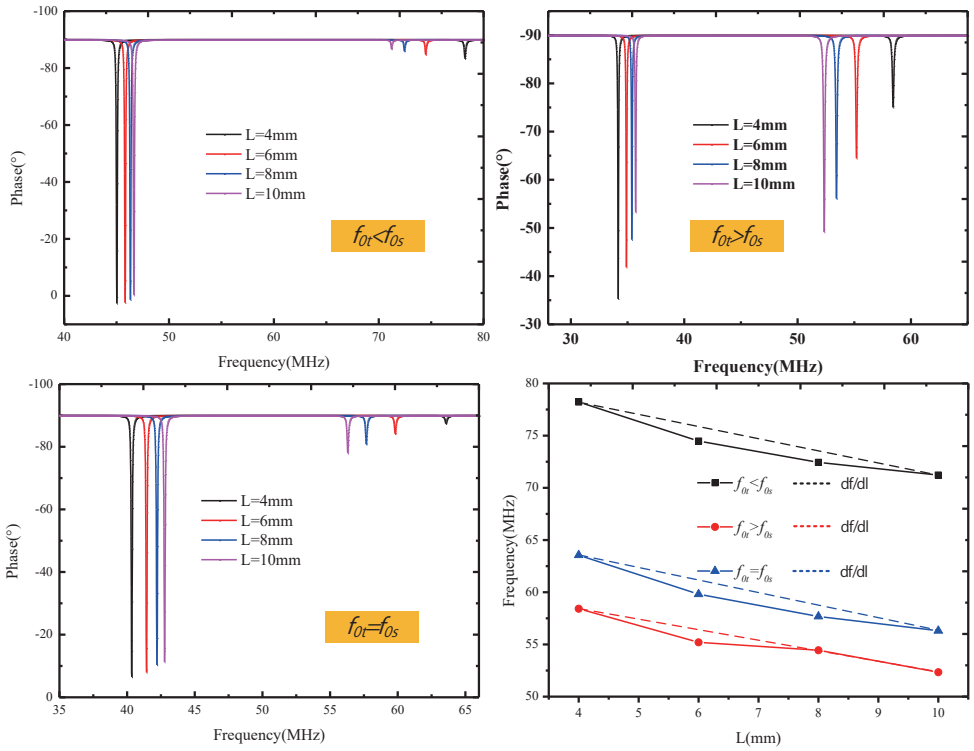

Fig. 5. (Color online) Theoretical analysis of the influence of k_{st} with $f_{0t} < f_{0s}$, $f_{0t} > f_{0s}$, and $f_{0t} = f_{0s}$.

Table 1
Parameters of sensor tag and transmitting coil.

Name	Description	Value
N_s/N_t	Number of turns	5
N_r	Number of turns	1
d_{out_t}/d_{out_s}	Length of outermost segment	40 mm
d_{out_r}	Length of outermost segment	30 mm
W	Conductor width	0.2 mm
S	Conductor spacing	0.2 mm
T	Conductor thickness	0.035 mm
L	Distance between sensor and antenna	Variable from 3 to 10 mm

to the parameters in Table 1, the mutual inductance M_{st} of the two coils obtained using the software auxiliary calculation is 0.573 μH. When the distance changes, the mutual inductance also changes. The mutual inductance M_{sr}, M_{rt} can be analyzed in the same way.

The system, which has the same parameter configuration as the system simulated by ADS software, was fabricated using printed circuit board (PCB) technology. Figure 6 shows the experimental setup of the system. The stationary part and sensor tag were stuck on two slide blocks that can move along the graduated side rail. The higher negative peak frequency was recorded when the relative distance of the sensor tag and stationary part increased from 3 to 10 mm, owing to the limited experimental equipment. The experimental results are illustrated in Fig. 7. The phase peaks illustrated in Fig. 8(a) correspond to the resonant characteristic of the transmitting coil with different distances away from the sensor tag. From Fig. 8(b), it is obvious

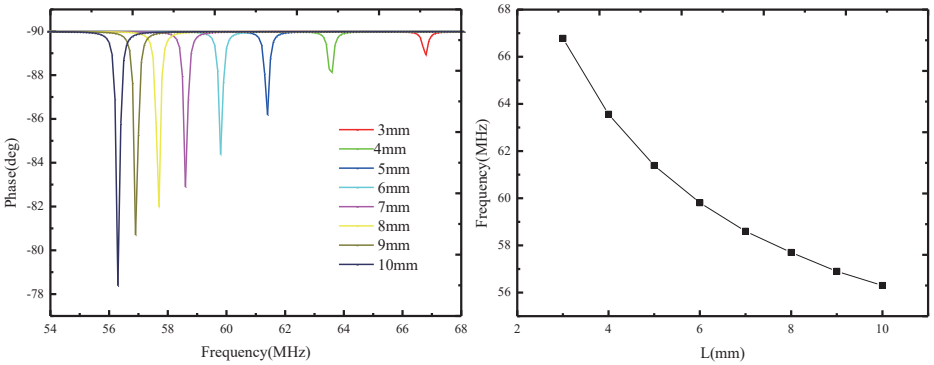

Fig. 6. (Color online) Electromagnetic simulation results obtained using ADS software.

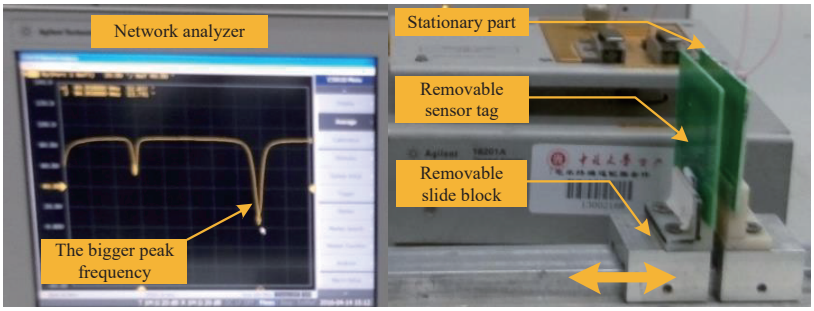

Fig. 7. (Color online) Tentative experimental setup of the proposed scheme.

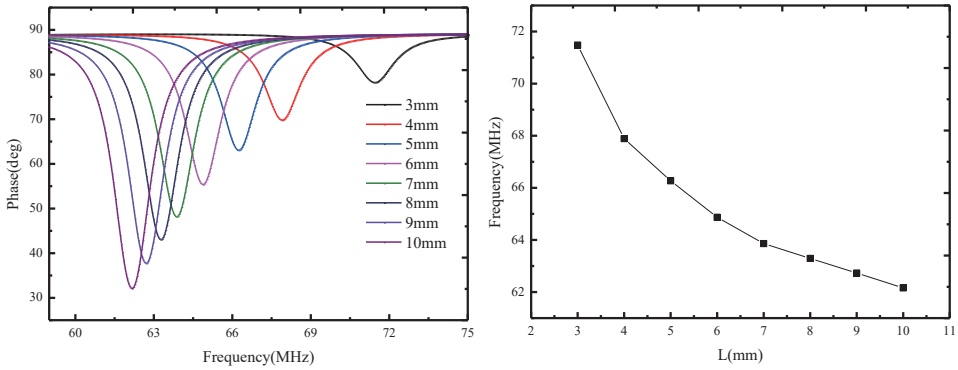

Fig. 8. (Color online) Experimental results. (a) Phase curves of the reader antenna with different relative positions of the stationary part and sensor tag. (b) Higher peak frequency versus distance.

that the peak frequency decreases from 71.48 to 62.15 MHz when the distance between the tag and stationary part changes from 10 to 3 mm. The experimental average sensitivity is derived up to 1.5 MHz/mm, which demonstrates the prospect of using this method to fulfill high-resolution displacement sensing in some industrial applications.

The measured frequency variation range in experiment is close to that in the theoretical analysis and electromagnetic simulation with $f_{0t} = f_{0s}$, which could be due to the proper construction of the multiple-coil coupling model. The coupling coefficient used in the theories and the simulation is the same. The magnetic-field strength between coils is nearly in inverse

ratio with the cube of the gap, so when two coils become close to each other, the coupling coefficient k_{st} increases rapidly especially beyond the yielding point. It is seen in Fig. 7(a) that the higher peak frequency decreases rapidly when the two coils become close together. The coupling model still has some deficiencies, such as the disregarding of the reader antenna's parasitic capacitance in the theoretical analysis and the neglect of the substrate material in ADS simulation. These factors also affect the performance of the sensor.

4. Conclusion

In this paper, we proposed a scheme for displacement measurement, which transforms the change displacement into the variation of the impedance characteristic frequency in the antenna port. The circuit model of the sensing system was first formulated theoretically and analyzed combined with MATLAB; then, electromagnetic simulation with the ADS software was performed. Both sets of the results demonstrated the feasibility of the proposed scheme. Finally, experiments were conducted to verify the above analysis. On the basis of the results of the mathematical analysis, simulation, and tentative experiments, it is likely that the proposed measurement scheme will find a place in applications where precise displacement measurement is needed.

Acknowledgments

This work was supported by the National Natural Science Foundation of China (Nos. 61471324 and 51425505) and the Program for the Top Young Academic Leaders of Higher Learning Institutions of Shanxi Province, China and sponsored by the Fund for Shanxi '1331 Poject' Key Subject Construction.

References

1 N. Misron, L. Q. Ying, R. N. Firdaus, N. Abdullah, N. F. Mailah, and H. Wakiwaka: Sensors **11** (2011) 10522.
2 J. W. Park, S. H. Sim, and H. J. Jung: Smart Mater. Struct. **23** (2014) 045022.
3 C. Paggi, C. Occhiuzzi, and G. Marrocco: IEEE T. Antennas Propag. **62** (2014) 905.
4 P. H. Lo, S. H. Tseng, J. H. Yeh, and W. Fang: Micromech. and Microeng. **23** (2013) 035013.
5 N. Y. Shentu, H. J. Zhang, Q. Li, and H. L. Zhou: IEEE Sens. J. **11** (2011) 1504.
6 B. Ozbey, E. Unal, H. Ertugrul, O. Kurc, C. M. Puttlitz, V. B. Erturk, A. Altintas, and H. V. Demir: Sensors **14** (2014) 1691.
7 N. Jeranče, D. Vasiljević, N. Samardžić, and G. Stojanović: Sensors **12** (2012) 1288.
8 H. R. Koo, Y. J. Lee, S. Gi, S. Khang, J. H. Lee, J. H. Lee, M. G. Lim, H. J. Park, and J. W. Lee: J. Med. Syst. **38** (2014).
9 H. B. Wang, B. Ju, W. Li, and Z. H. Feng: Sens. Actuators, A **211** (2014) 98.
10 S. M. Djuric: IEEE T. Magn. **50** (2014) 4004104.
11 A. J. Fleming: Sens. Actuators, A **190** (2013) 106.
12 D. A. Sanz, C. Mitrosbaras, E. A. Unigarro, and F. S. Quijano: Appl. Phys. Lett. **103** (2013).
13 C. Zhang, J. Q. Huang, and Q. A. Huang: 8th IEEE Int. Conf. Nano/Micro Engineered and Molecular Systems (NEMS) (2013) 256.
14 U. M. Jow and M. Ghovanloo: J. IEEE Trans. Biomed. Circuits Syst. **1** (2007) 193.
15 M. A. Fonseca: Dissertations & Theses—Gradworks (Georgia Institute of Technology, Atlanta, 2007).